Supporting Information for

Graphene Oxide-regulated Hydrogel Membrane for Extreme Heavy Metal Recovery: The Role of Size Exclusion and Ultralong Three-dimensional Channel Adsorption

Xin Mao[b,a], Bin Liu[a]*, Bing Zhang[c]*, Chunzhao Chen[a], Qianxin Zhang[a], Shan Niu[a]

[a] *School of Technology for Sustainability, Advanced Interdisciplinary Institute of Environment and Ecology, Guangdong Provincial Key Laboratory of Wastewater Information Analysis and Early Warning, Beijing Normal University, Zhuhai 519087, China*

[b] *Hunan Engineering Research Center of Water Security Technology and Application, College of Civil Engineering, Hunan University, Changsha 410082, PR China*

[c] *National Research Base of Intelligent Manufacturing Service, Chongqing Technology and Business University, Chongqing 400067, China*

*Corresponding author.

Tel.: +86 451 86282252; Fax: +86 451 86282252.

E-mail address:

ahxclb@163.com (Bin Liu)

Text S1. Determination of Transmembrane Energy Barriers for Heavy Metals.

The energy barrier for the permeation (E_p, kJ/mol) of heavy metal ions infiltrated into NF membranes was determined using the Arrhenius relationship.[1,2]

$$\ln\left(\frac{J_s}{c_m - c_p}\right) = \ln J_p - \left(\frac{E_p}{R} \times \frac{1}{T}\right) \quad \text{(S1)}$$

Where J_s represents solution flux (mol/m^2·h); c_m and c_p denote the concentrations of heavy metals on the membrane surface and effluent (mol/L), respectively. J_p is the pre-exponential indicator; R and T represent the ideal gas constant (8.314 J/mol·K) and absolute temperature (K), respectively.

The solution flux (J_s, mol/m^2·h) was calculated using Eq. (S2).

$$J_s = J_v \times c_p \quad \text{(S2)}$$

where J_v is the volumetric flux (L/m^2·h) and c_p is the heavy metal concentration (mol/L). c_p was taken at the late stages of filtration (permeate volume between 500 and 600 mL) to ensure that the measured J_s is a representative case of steady-state conditions (after the observed breakthrough).

The heavy metal concentration at the membrane surface (c_m, mg/L) was calculated using the stagnant film model (Eq.(S3)), where the longitudinal mass transport within the boundary layer adjacent to the membrane surface is assumed negligible,[2] and hence, the mass transport within the membrane is considered one-dimensional (perpendicular towards the membrane surface).

$$c_m = c_r\left(\left(1 - R_{obs}\right) + R_{obs}e^{\frac{J_v}{k_m}}\right) \quad \text{(S3)}$$

where k_m is the heavy metal mass transfer coefficient from the feed solution towards the membrane surface (m/s). The mass transfer coefficient depends on the Reynolds number (that is related to the stirrer speed and system geometry) and the solution properties (solute diffusivity in water, water density, and viscosity) given in terms of the Schmidt number.[3]

The heavy metal observed retention (R_{obs}) was calculated with Eq. (S4)

$$R_{obs} = 1 - \frac{c_p}{c_r} \quad \text{(S4)}$$

where c_p and c_r are the heavy metal concentration (mg/L) in the permeate and retentate, respectively.

The mass transfer coefficient of heavy metal was calculated based on the diffusion coefficient in water (D_w), Reynolds number (R_e), Schmidt number (S_c), and Sherwood correlation (Sh).[2–5]

$$Sh = \frac{k_m d_h}{D_w} = a {R_e}^b {S_c}^c \quad \text{(S5)}$$

$$Sh = 1.86(R_e S_c \frac{d_h}{L})^{0.33} \quad (L > L^*) \quad \text{(S6)}$$

$$Sh = 0.664 {R_e}^{0.5} (S_c \frac{d_h}{L})^{0.33} \quad (L < L^*) \quad \text{(S7)}$$

$$Sh = 1.62(R_e S_c \frac{d_h}{L})^{0.33} \quad (100 < R_e S_c \frac{d_h}{L} < 5000) \quad \text{(S8)}$$

where d_h is the hydraulic diameter of the flow channel (m), and L is the characteristic length of the channel (m). L^* (m) is the distance from the channel inlet where the velocity profile is completely developed ($= 0.029 d_h R_e$).

Text S2. Determination of MWCO and Pore Size Distribution

The MWCO of the PAM/SA/Mxene membranes was determined by a standard method of measuring the rejection of neutral molecules, such as glycerol (92 Da), xylose (120 Da), glucose (180 Da), and sucrose (342 Da), by the membranes. The aqueous solution of these neutral molecules with a concentration of 200 ppm was used as feed to pass through the membrane at 4 bar. The rejection of neutral molecules was calculated according to the concentration of the feed and permeate qualified by total organic carbon. The MWCO of the membranes was equal to the molecular weight of the neutral molecule with a rejection of 90%.

With the premise of no steric and hydrodynamic interactions between these neutral solutes and the pores of the membranes, the corresponding pore size distribution can be expressed by the probability density function (Eq. (S9)).

$$\frac{dR(d_p)}{dd_p} = \frac{1}{d_p ln\sigma_p \sqrt{2\pi}} exp[-\frac{(lnd_p - ln\mu_p)^2}{2(ln\sigma_p)^2}] \quad \text{(S9)}$$

where d_p is the stokes diameter of the neutral molecules, μ_p is the mean pore size and σ_p is the geometric standard deviation of the probability density function curve. The μ_p is equals to the d_p of the neutral solute with a rejection of 50%. σ_p represents the distribution of the membrane pore size, which is the ratio of d_p of the neutral molecule with a rejection of 84.13% to that of 50%. The d_p of the neutral solutes is calculated according to Eq. (S10).

$$lg\frac{d_p}{2} = -1.4962 + 0.4654lgM \quad \text{(S10)}$$

The pore size range of PAM/SA/Mxene membranes is determined from the probability density function curve using the data extraction tool (Getdata), where all pores with probability density greater than 0.01 in the curve are included to determine the distribution range of pore size from minimum to maximum.

Text S3. Characteristics of IPN/GO Membrane

Scanning electron microscopy (SEM; QUANTA200, FEI, Netherlands) and atomic force microscopy (AFM; Dimension ICON, Bruker, Germany) were utilized to characterize the hydrogel channels and surface morphology of the IPN/GO membrane.[6] X-ray photoelectron spectroscopy (XPS; Thermo ESCALAB 250Xi, Thermo Fisher Scientific; America) and Fourier transform infrared spectroscopy (FTIR; Bruker Co., Germany) were employed to elucidate the cross-linking characteristics and chemical composition of the hydrogel layer. Time-of-flight secondary ion mass spectrometry (TOF-SIMS; ION-ToF GmbH, Germany) was used for the qualitative assessment of the adsorption levels and distribution of heavy metal ions within the hydrogel channels.[7] Additionally, the contact angle and zeta potential of various IPN/GO gel membranes were measured to elucidate the hydrophilicity and charge density of the hydrogel channels.

Text S4. Ion Adsorption Test

The ion adsorption performance of the prepared IPN/GO hydrogel membrane was evaluated through a salt separation process. Before the actual testing, the hydrogel membrane was compacted for one hour under a pressure of 2 bar to achieve stable permeability. During the experiment, the transmembrane pressure was

maintained at 4 bar. Filtration adsorption experiments were conducted with 1000 ppm of $CuSO_4$ used individually as the feed solution, with a runtime of 2 hours. After filtration, the hydrogel membrane was placed in a water environment at 90°C to dissolve and desorb, and the amount of Cu^{2+} adsorbed was determined by inductively coupled plasma spectroscopy (ICP, Agilent 5100, Bruke).

REFERENCES

(1) Epsztein, R.; DuChanois, R. M.; Ritt, C. L.; Noy, A.; Elimelech, M. Towards Single-Species Selectivity of Membranes with Subnanometre Pores. *Nat. Nanotechnol.* **2020**, *15* (6), 426–436. https://doi.org/10.1038/s41565-020-0713-6.

(2) Allouzi, M.; Imbrogno, A.; Schäfer, A. I. Energy Barriers for Steroid Hormone Transport in Nanofiltration. *Environ. Sci. Technol.* **2022**, *56* (23), 16811–16821. https://doi.org/10.1021/acs.est.2c04658.

(3) Imbrogno, A.; Schäfer, A. I. Comparative Study of Nanofiltration Membrane Characterization Devices of Different Dimension and Configuration (Cross Flow and Dead End). *J. Memb. Sci.* **2019**, *585* (April), 67–80. https://doi.org/10.1016/j.memsci.2019.04.035.

(4) Zhai, X.; Wang, Y. L.; Dai, R.; Li, X.; Wang, Z. Roles of Anion-Cation Coupling Transport and Dehydration-Induced Ion-Membrane Interaction in Precise Separation of Ions by Nanofiltration Membranes. *Environ. Sci. Technol.* **2022**, *56* (19), 14069–14079. https://doi.org/10.1021/acs.est.2c04772.

(5) van den Berg, G. B.; Rácz, I. G.; Smolders, C. A. Mass Transfer Coefficients in Cross-Flow Ultrafiltration. *J. Memb. Sci.* **1989**, *47* (1–2), 25–51. https://doi.org/10.1016/S0376-7388(00)80858-3.

(6) Dong, J.; Zhang, Z.; Yu, Z.; Dai, X.; Xu, X.; Alvarez, P. J. J.; Zhu, L. Evolution and Functional Analysis of Extracellular Polymeric Substances during the Granulation of Aerobic Sludge Used to Treat P-Chloroaniline

Wastewater. *Chem. Eng. J.* **2017**, *330*, 596–604. https://doi.org/10.1016/J.CEJ.2017.07.174.

(7) Mao, X.; Cai, J.; Xie, F.; Yan, P.; Liu, B. Effect of Peroxydisulfate Activated by B-Doped NiFe2Ox for Degrading Contaminants and Mitigating Nanofiltration Membrane Fouling in the Landfill Leachate Treatment. *J. Hazard. Mater.* **2024**, *480* (September), 136239. https://doi.org/10.1016/j.jhazmat.2024.136239.

(8) Tortora, F.; Innocenzi, V.; Prisciandaro, M.; Vegliò, F.; Mazziotti di Celso, G. Heavy Metal Removal from Liquid Wastes by Using Micellar-Enhanced Ultrafiltration. *Water. Air. Soil Pollut.* **2016**, *227* (7). https://doi.org/10.1007/s11270-016-2935-7.

(9) Li, X.; Zhang, C.; Zhang, S.; Li, J.; He, B.; Cui, Z. Preparation and Characterization of Positively Charged Polyamide Composite Nanofiltration Hollow Fiber Membrane for Lithium and Magnesium Separation. *Desalination* **2015**, *369*, 26–36. https://doi.org/10.1016/j.desal.2015.04.027.

(10) Hosseini, S. S.; Nazif, A.; Alaei Shahmirzadi, M. A.; Ortiz, I. Fabrication, Tuning and Optimization of Poly (Acrilonitryle) Nanofiltration Membranes for Effective Nickel and Chromium Removal from Electroplating Wastewater. *Sep. Purif. Technol.* **2017**, *187*, 46–59. https://doi.org/10.1016/j.seppur.2017.06.018.

(11) Linde, K.; Jönsson, A. S. Nanofiltration of Salt Solutions and Landfill Leachate. *Desalination* **1995**, *103* (3), 223–232. https://doi.org/10.1016/0011-9164(95)00075-5.

(12) Chaudhari, L. B.; Murthy, Z. V. P. Treatment of Landfill Leachates by Nanofiltration. *J. Environ. Manage.* **2010**, *91* (5), 1209–1217. https://doi.org/10.1016/j.jenvman.2010.01.007.

(13) Zhang, Y.; Zhang, S.; Chung, T. S. Nanometric Graphene Oxide Framework Membranes with Enhanced Heavy Metal Removal via Nanofiltration. *Environ. Sci. Technol.* **2015**, *49* (16), 10235–10242. https://doi.org/10.1021/acs.est.5b02086.

(14) Gao, J.; Sun, S. P.; Zhu, W. P.; Chung, T. S. Green Modification of Outer Selective P84 Nanofiltration (NF) Hollow Fiber Membranes for Cadmium Removal. *J. Memb. Sci.* **2016**, *499*, 361–369. https://doi.org/10.1016/j.memsci.2015.10.051.

(15) Cheng, X.; Zhang, Y.; Shao, S.; Lai, C.; Wu, D.; Xu, J.; Luo, X.; Xu, D.; Liang, H.; Zhu, X. Highly Permeable Positively Charged Nanofiltration Membranes with Multilayer Structures for Multiple Heavy Metal Removals. *Desalination* **2023**, *548* (September 2022), 116266. https://doi.org/10.1016/j.desal.2022.116266.

(16) Xu, Y. C.; Wang, Z. X.; Cheng, X. Q.; Xiao, Y. C.; Shao, L. Positively Charged Nanofiltration Membranes via Economically Mussel-Substance-

Simulated Co-Deposition for Textile Wastewater Treatment. *Chem. Eng. J.* **2016**, *303*, 555–564. https://doi.org/10.1016/j.cej.2016.06.024.

(17) Xu, S. J.; Shen, Q.; Luo, L. H.; Tong, Y. H.; Wu, Y. Z.; Xu, Z. L.; Zhang, H. Z. Surfactants Attached Thin Film Composite (TFC) Nanofiltration (NF) Membrane via Intermolecular Interaction for Heavy Metals Removal. *J. Memb. Sci.* **2022**, *642* (July 2021), 119930. https://doi.org/10.1016/j.memsci.2021.119930.

(18) Gao, J.; Wang, K. Y.; Chung, T. S. Design of Nanofiltration (NF) Hollow Fiber Membranes Made from Functionalized Bore Fluids Containing Polyethyleneimine (PEI) for Heavy Metal Removal. *J. Memb. Sci.* **2020**, *603* (February). https://doi.org/10.1016/j.memsci.2020.118022.

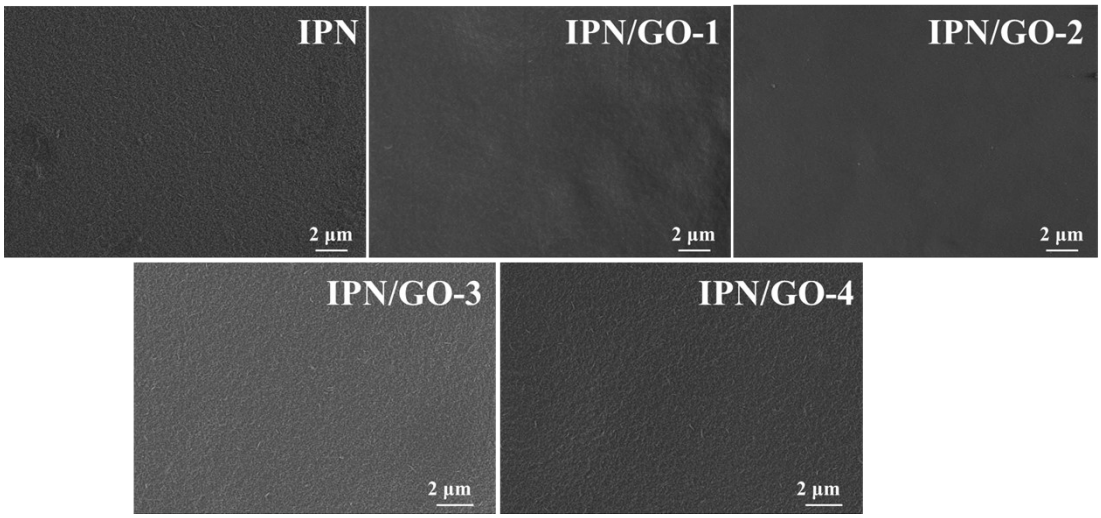

Figure S1. SEM images of IPN and IPN/GO-1, 2, 3, and 4 hydrogel membrane surface.

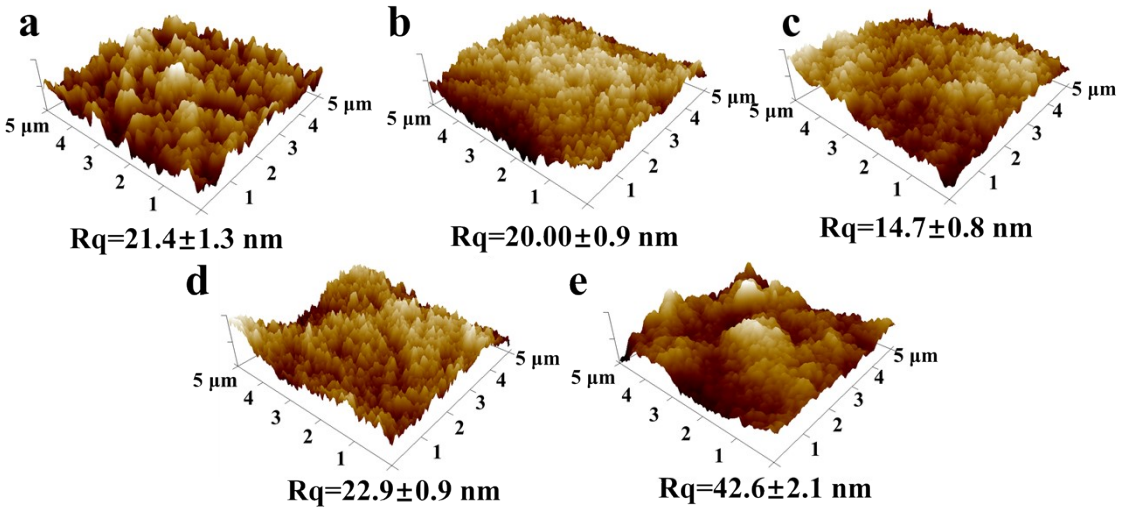

Figure S2. AFM images of IPN and IPN/GO-1, 2, 3, and 4 hydrogel membrane surface. a, b, c, d, and e represent IPN and IPN/GO-1, 2, 3, and 4 hydrogel membranes, respectively.

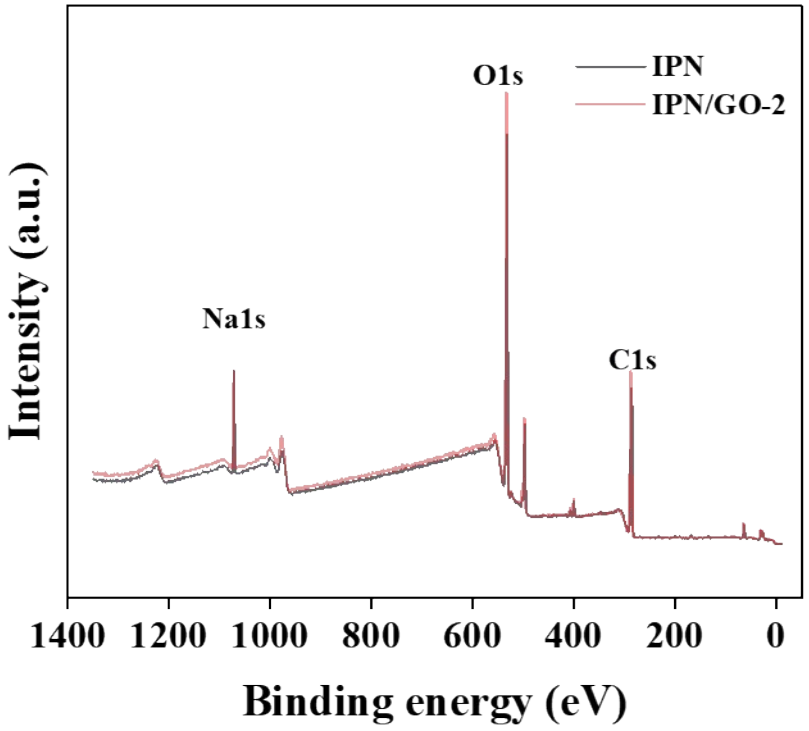

Figure S3. XPS spectra of IPN and IPN/GO-2 hydrogel membranes.

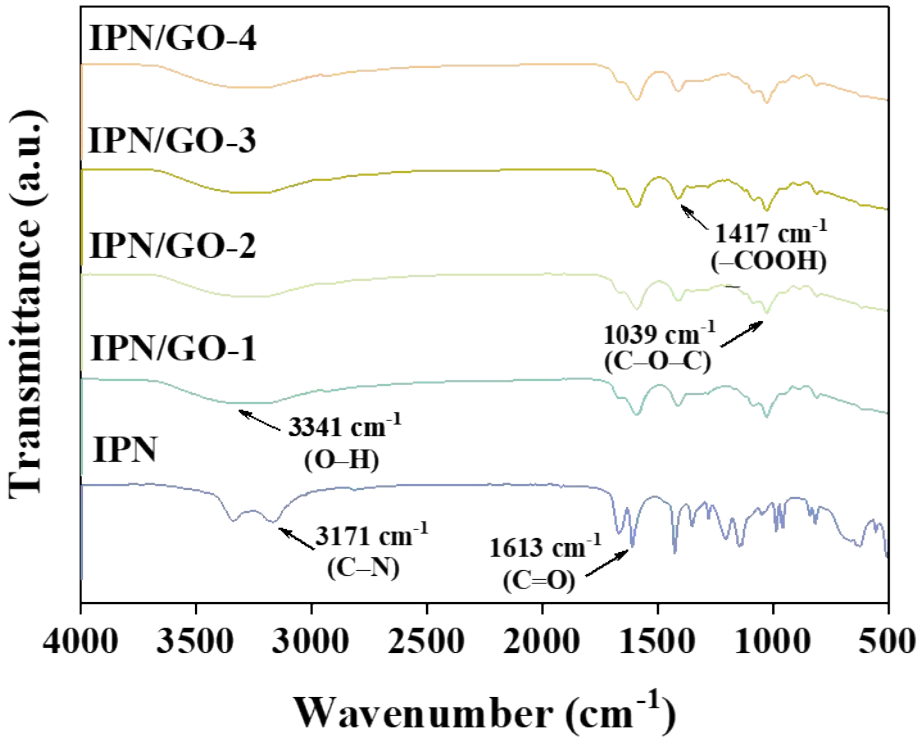

Figure S4. FTIR spectra of IPN and IPN/GO-1, 2, 3, and 4 hydrogel membrane surface.

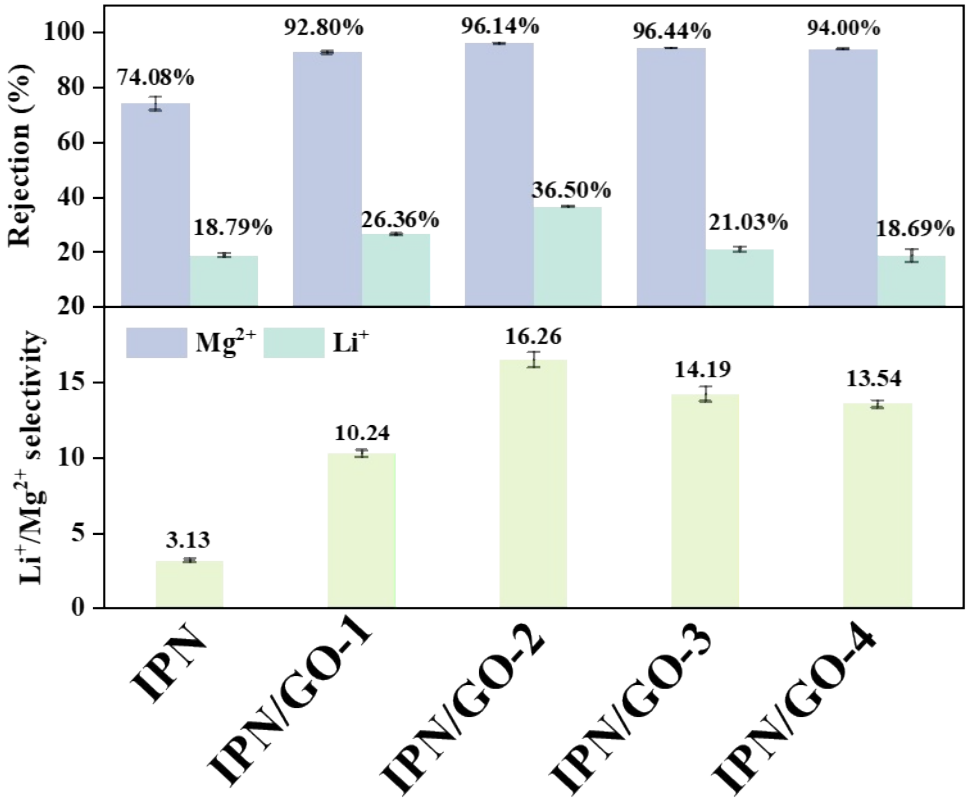

Figure S5. The rejection efficiencies of Mg^{2+} and Li^{+} and the selectivity of Mg^{2+}/Li^{+} vary with the change in the mass ratio of Mg^{2+}/Li^{+} (feed solution salt concentration was 2000 ppm).

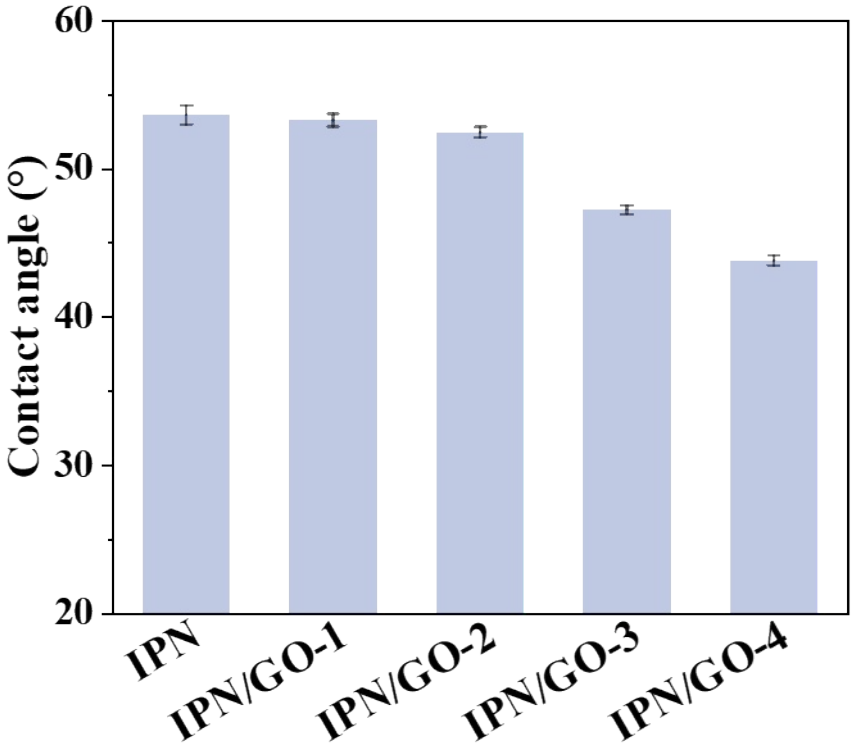

Figure S6. The pure water contact angles of different IPN/GO hydrogel membranes.

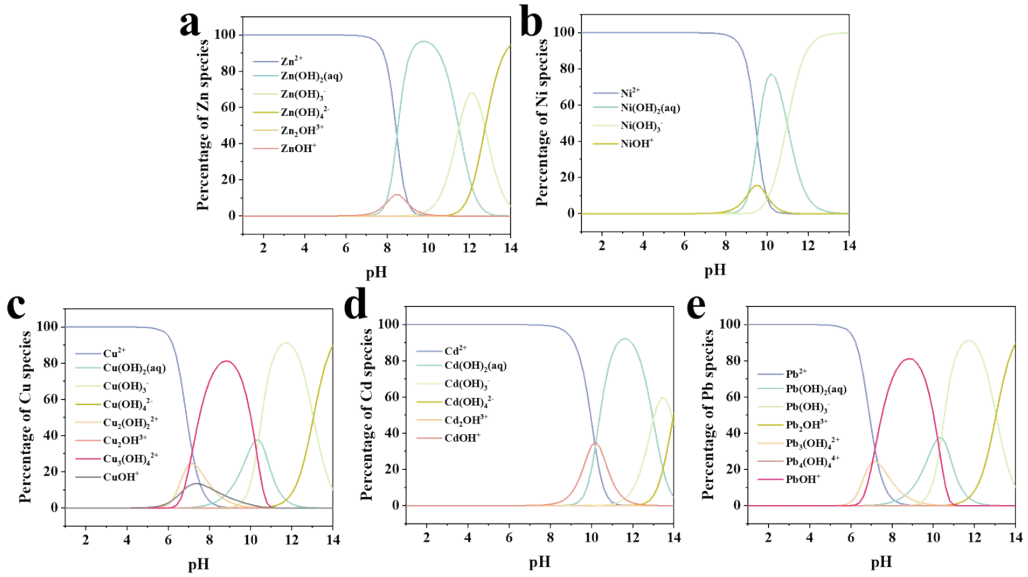

Figure S7. Existing forms of heavy metal ions in the feed solution under an equilibrium state using Visual MINTEQ software simulation.

Table S1 Summary of heavy metal recovery efficiency of IPN/GO membrane and previously reported membranes.

Membrane methods	Types of heavy metals	Trans-membrane pressure	Feed concentration	Recovery efficiency	Flux (LMH/bar)	Reference
IPN/GO	Zn^{2+}, Ni^{2+}, Cu^{2+}, Cd^{2+}, and Pb^{2+}	3 bar	1000 ppm	>91.38%	7.82	★This work
IPN/GO (Adjust pH to 11)	Zn^{2+}, Ni^{2+}, Cu^{2+}, Cd^{2+}, and Pb^{2+}	3 bar	1000 ppm	>98.87%	7.82	★This work
MEUF +SDS surfactant	Co^{2+}, Ni^{2+}, Cr^{3+}, and Zn^{2+}	2.8 bar	10 ppm	>79%	~71.43	[8]
NF270	Ni^{2+} and Cu^{2+}	5 bar	20 ppm	>65%	13.8	[9]
PAN-NF membrane	Ni^{2+} and $Cr_2O_7^{2-}$	10 bar	50 ppm	>82.3%	7.18	[10]
AFC30	Zn^{2+}, $Ni^{2+}$and Pb^{2+}	15 bar	0.495 ppm;0.016 ppm; 0.609 ppm	>88.3%	2.33	[11]

NF300	Ni and Cr	8 bar	-	>55%	8.75	[12]
GO&EDA_HPEI 60K	Zn^{2+}, Ni^{2+}, Cd^{2+}, and Pb^{2+}	1 bar	1000 ppm	>90.50%	5.0	[13]
M-PEI&GA	Cd^{2+}	5 bar	1000 ppm	94.0%	1.7	[14]
CS-P/T-PEI	Mn^{2+}, Ni^{2+}, Cu^{2+}, Cd^{2+}, and Pb^{2+}	4 bar	500 ppm	89.2%	10.9	[15]
Catechol-PEI/PAN	Cu^{2+}	5 bar	2000 ppm	~84%	2.6	[16]
Surfactant attached NF membrane	Ni^{2+}, Cu^{2+}, and Pb^{2+}	3.5 bar	1000 ppm	>80%	~21.0	[17]
Plain_TMC10	Ni^{2+}, Cu^{2+}, and Zn^{2+}	1.0 bar	1000 ppm	>92%	~5.0	[18]

Table S2 Physical properties of various heavy metal ions used in this work.

Ion species	Hydrated diameter (Å)	Diffusivity (10^{-9} $m^2 \cdot s^{-1}$)
Zn^{2+}	8.60	0.71
Ni^{2+}	8.08	0.68
Cu^{2+}	8.38	0.72
Cd^{2+}	8.52	0.87
Pb^{2+}	8.02	0.95